POLITECNICO DI TORINO
Repository ISTITUZIONALE

Photonic Interferometric Imager with monolithic silicon CMOS photonic integrated circuits

(Article begins on next page)

29 November 2022

Photonic Interferometric Imager with monolithic silicon CMOS photonic integrated circuits

Humphry Chen, Mehmet Berkay On, Yun-Jhu-Lee, Li Zhang, Roberto Proietti, and S.J. Ben Yoo

Department of Electrical and Computer Engineering, University of California, Davis, One Shields Ave, Davis California 95616 USA

sbyoo@ucdavis.edu

Abstract: We demonstrate, for the first time to our knowledge, a monolithically-integrated photonic interferometric imager circuit with on-chip detectors, CMOS trans-impedance-amplifiers, and associated photonic imager components. A proof-of-principle demonstration of interferogram fringe generation will be discussed. © 2022 The Authors

1. Introduction

Traditional imaging systems require relatively bulky lenses or mirrors to directly collect light from remote objects onto detector arrays. A high-resolution imaging system requires proportionally large lenses and mirrors in a large housing together with a detector array to hold the entire system aligned in place overcoming temperature variations and mechanical vibrations. On the other hand, interferometric imaging can overcome the requirement for large lenses or mirrors by utilizing many (*N*) subapertures and by reconstructing the image by utilizing van Cittert-Zernike theorem. Recently, the Event Horizon Telescope utilized multiple mm-wave telescopes across the globe as a very-long baseline interferometer (VLBI) system to create the first images of the black hole [1], and Berkley infrared spatial interferometer utilized heterodyne at 11 μm wavelengths to achieve high-resolution imaging [2]. The common challenges to the interferometric imaging using such subaperture optics are (1) scalability: how to scale the number of subapertures to a large number in the (u,v) plane so that the image reconstruction can be realized without having to move the subapertures and (2) stability: how to keep such subapertures in interfrometricly fixed locations so that image reconstruction can be achieved. More recently, Segmented Planar Imaging Detector for Electro-optical Reconnaissance (SPIDER) imager utilizing photonic integrated circuits (PICs) have been proposed [3] and demonstrated [4]. PIC based imagers are attractive since they offer scalability and stability on a monolithic platform. The previous SPIDER PIC demonstrations required off-chip detection and signal amplification [4]. In this paper, we exploit monolithic silicon CMOS photonic platform [5] (GF9WG) to realize a 9-baseline interferometric imager PIC with integrated spectrometers, tunable Mach-Zehnder interferometers, optical hybrids, balanced photodiodes, and transimpedance amplifiers (TIAs).

2. Photonic Interferometry for Fourier domain imaging

Figure 1 (a) shows a schematic for a PIC based interferometric imager for an arbitrary number of baselines. The incoming light is vertically coupled into the grating couplers on the left side of the PIC in Figure 1. The input grating couplers are divided into multiple pairs to create multiple baseline lengths. The interferometer design is fabricated in a 1.7 mm× 5 mm area by a commercial foundry (see Figure 1 (b)), where nine baselines are integrated with CMOS electronics. The input gratings are spaced by 250 μm skipping a grating in the center of the PIC, allowing for the light to be coupled into the PIC using an angled fiber array. Each grating pair within the PIC combines each input's light into a 2 × 2 coupler. The output of one of the coupler ports is given by $P_{out} = P_1 + P_2 + 2\sqrt{P_1 P_2}\cos(\Delta\Phi)$, where P_1 and P_2 represent the optical power coming from each arm of the baseline. The outputs of the 2 × 2 couplers are connected to demux circuits, designed using asymmetric Mach-Zehnders. These wavelength demux blocks are designed to split up to two wavelengths from the optical inputs with a wavelength spacing of 50 nm. Each wavelength output is path length matched as they are routed to the balanced detectors. The balanced detectors measure the interference fringes on the output as the phase shifters are tuned for each arm. The outputs of the detectors are amplified by the trans-impedance amplifiers (TIAs) placed directly after the detectors. The TIA is designed to have a gain of 40 dBohm, amplifying across a 10 GHz bandwidth, which is within the balanced detectors' electrical bandwidth.

For each baseline pair, the balanced detector output is given by $I_{BPD} = 2R\sqrt{P_1 P_2}\cos(\Delta\Phi)$, where $\Delta\Phi$ is the phase difference between the arms of the baseline and R is the responsivity of the photodetectors. The phase difference term includes both the path mismatch of the input signals along with the phase tuning of each arm in the baseline. As the phase shifters are tuned, the output signal will oscillate for values of $\Delta\Phi$ between 0 and 2π depending on how the input

signals interfere with one another. Thus, the output signals can be used to acquire the Fourier domain information of the image source for each baseline based on the phase tuning.
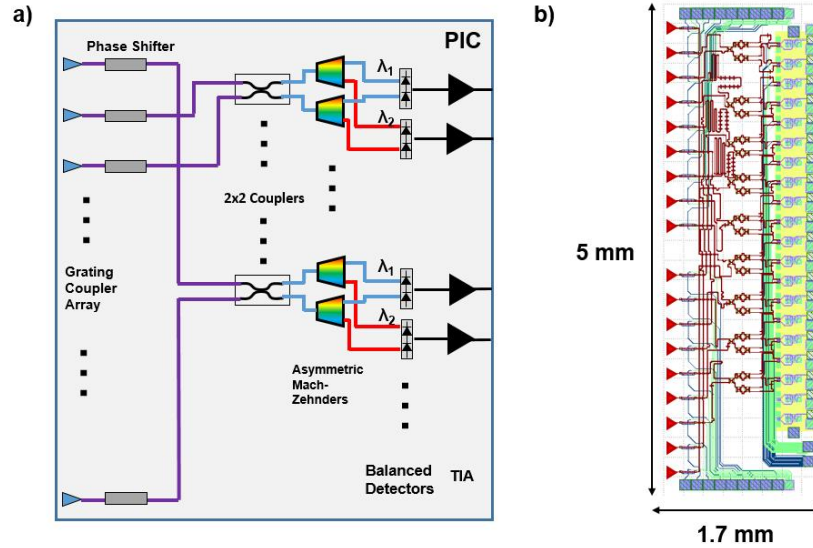

Figure 1. (a) A generalized schematic design of an interferometric imager PIC including onchip grating couplers, phase-shifters, 2x2 couplers, balanced photodetectors, and transimpedance amplifiers (b) a monolithic interferometric imager chip layout hat follows the general schematic in (a). The grating inputs are designed to have 250 μm spacing which allows for a fiber array to be coupled in.

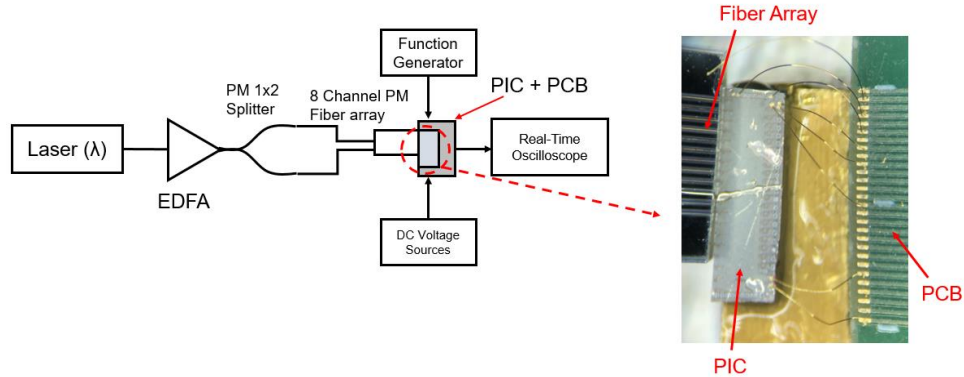## 3. Experimental Results and Discussions

Figure 2. Experimental diagram of proof-of-concept measurement for the PIC with a picture of the edge coupling part of the setup. To maximize the coupling, the fiber array is mounted on a 3-axis stage and 2-angle stage. The PIC is wire-bonded onto a PCB with connections to the phase shifters and detector circuit for the single baseline.. The detectors and TIA are biased separately to maximize the detected signal.

For a proof-of-principle demonstration, we started by coupling a single wavelength signal into the shortest baseline of the PIC and tuned the phase of one of the baseline arms, as shown in Figure 2. This experiment is used to determine the effectiveness of the design and the operating conditions needed to create interference fringes within the PIC. In addition, the input signal is a single wavelength, which is sufficient to observe an interference fringe as the phase shifter is tuned. Due to the edge coupling setup, the signal is fed into an EDFA to compensate for extra loss introduced from coupling the fiber array to the PIC. The full experiment will not require an EDFA to couple the light into the grating inputs. The paths after the 1 ×2 coupler are minimized to reduce the phase fluctuation introduced by the fiber optic components. In this experiment, the path length-matched inputs allow for the characterization of the phase shifter's tuning range and capabilities to generate an interferometric fringe.

The phase is tuned using a function generator that applies a voltage that linearly sweeps from 0 to π phase shift and from π to 0 phase shift. As the phase tuning function progresses, as shown in Figure 3 (a), the signal output is measured to observe the amplitude change in the signal. For this experiment, the signal is modulated with a square wave using the laser's internal modulator to help observe the effects of the phase tuning on the signal output. Figure 3 (b) shows that the introduction of the optical signal into the system decreases the TIA output from the DC voltage term from

biasing the circuit. The highest power in the signal outputs occurs when the applied voltage to the phase shifter is 0 V, while the lowest power in the outputs occurs when the voltage is at 5V. Thus, the effects of the optical power into the system are reflected in millivolt changes in the TIA output. The millivolt output signal means that the optical power into the detector is approximately -40 dBm, which allows the system to detect and amplify weak optical signals without the use of external electrical amplifiers.
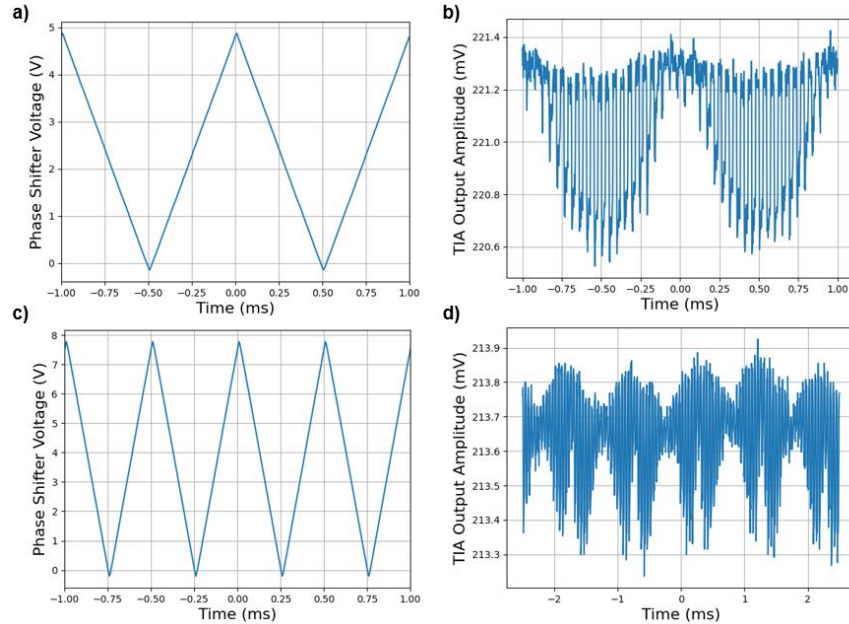

Figure 3. (a) Function Generator Output used to tune the phase shifter, (b) TIA output signal vs. time using a modulated signal, (c) Function Generator Output used to tune the phase shifter at a higher frequency, (d) TIA output signal vs. time with an additional phase shift added due to the fiber components.

For the results of Figure 3 (c, d), we tuned the phase shifter using a waveform that has a higher frequency while an extra phase shift is introduced in the fiber components for the input signal. This extra phase shift will cause the TIA output to have some level of interference between the baseline arms, which is exaggerated with the phase shifter's tuning. This indicates that the phase shifters are operating correctly and creating a delay between baseline arms.

4. Conclusion

We demonstrated a monolithic interferometer device and tested it with a proof-of-concept single baseline experiment. Future studies will aim to capture data across multiple baselines and reconstruct the source image across multiple lighting scenarios.

5. References

[1]   K. Akiyama, A. Alberdi, W. Alef, K. Asada, R. Azulay, A.-K. Baczko, … , and L. Ziurys, "First M87 Event Horizon Telescope Results. II. Array and Instrumentation," *Astrophys. J.*, vol. 875, no. 1, p. L2, 2019, doi: 10.3847/2041-8213/ab0c96.

[2]   D. D. S. Hale, M. Bester, W. C. Danchi, W. Fitelson, S. Hoss, E. A. Lipman, J. D. Monnier, P. G. Tuthill, and C. H. Townes, "The Berkeley Infrared Spatial Interferometer: A Heterodyne Stellar Interferometer for the Mid-Infrared," *Astrophys. J.*, vol. 537, no. 2, pp. 998–1012, 2000, doi: 10.1086/309049.

[3]   A. L. Duncan and R. L. Kendrick, "Segmented planar imaging detector for electro-optic reconnaissance," US8913859B1, 2014.

[4]   T. Su, G. Liu, K. E. Badham, S. T. Thurman, R. L. Kendrick, A. Duncan, D. Wuchenich, C. Ogden, G. Chriqui, S. Feng, J. Chun, W. Lai, and S. J. B. Yoo, "Interferometric imaging using Si3N4 photonic integrated circuits for a SPIDER imager," *Opt. Express*, vol. 26, no. 10, pp. 12801–12812, 2018, doi: 10.1364/OE.26.012801.

[5]   K. Giewont, K. Nummy, F. A. Anderson, J. Ayala, T. Barwicz, Y. Bian, K. K. Dezfulian, D. M. Gill, T. Houghton, S. Hu, B. Peng, M. Rakowski, S. Rauch, J. C. Rosenberg, A. Sahin, I. Stobert, and A. Stricker, "300-mm Monolithic Silicon Photonics Foundry Technology," *IEEE J. Sel. Top. Quantum Electron.*, vol. 25, no. 5, pp. 1–11, 2019, doi: 10.1109/JSTQE.2019.2908790.